Structural Characterization of Manganese(II)−Nucleotide Complexes Bound to Yeast 3-Phosphoglycerate Kinase: ^{13}C Relaxation Measurements Using [U-^{13}C]ATP and [U-^{13}C]ADP†

Vidya Raghunathan,‡ Mei H. Chau, Bruce D. Ray, and B. D. Nageswara Rao*

Department of Physics, Indiana University−Purdue University Indianapolis (IUPUI), 402 North Blackford Street, Indianapolis, Indiana 46202-3273

Received June 16, 1999; Revised Manuscript Received September 8, 1999

ABSTRACT: A complete characterization of the conformations of Mn·ADP and Mn·ATP bound to the active site of yeast 3-P-glycerate kinase is presented. These conformations have been deduced on the basis of paramagnetic effects on ^{13}C spin−lattice relaxation rates in [U-^{13}C]nucleotides due to Mn(II), used as a substituent activating cation. The ^{13}C relaxation measurements were performed on exclusively enzyme-bound complexes E·Mn·[U-^{13}C]ATP and E·Mn·[U-^{13}C]ADP at three distinct ^{13}C NMR frequencies: 75.4, 125.7, and 181 MHz. The frequency dependence of the relaxation data has been analyzed in an effort to evaluate distances from the cation for all 10 ^{13}C nuclei in the adenosine moieties of E·Mn·ATP and E·Mn·ADP. These distance data, taken along with previously published cation−^{31}P distances, have been used as constraints in the molecular modeling program Quanta, in which molecular dynamics simulations and energy minimization have been performed to determine the conformations that are compatible with the distance data. It was possible to model the distances on the basis of a single enzyme-bound conformation for each of the nucleotides. The details of the enzyme-bound Mn·ATP and Mn·ADP conformations are distinguishably different from each other, indicating that structural alterations occur in the enzyme-bound reaction complex as the enzyme turns over. For example, when the adenosine moieties in the bound structures of Mn·ATP and Mn·ADP are superposed, the cation is found to be displaced by ∼2.4 Å between the two conformations, suggesting that these structural changes may involve movements with significant amplitudes. Furthermore, the NMR-determined structures of enzyme-bound Mn·ATP and Mn·ADP are significantly different from those in published X-ray crystal structures of the enzyme−nucleotide complexes.

ATP-utilizing enzymes, belonging to several categories such as phosphoryl transfer, adenylyl transfer, and pyrophosphoryl transfer, participate in a number of critical cellular processes. In vivo, these enzymes utilize Mg(II) for their activation, which may be substituted by the paramagnetic cations Mn(II) or Co(II) in vitro. This substitution allows the determination of the structure of the enzyme-bound substrates through measurements of distance-dependent enhancement of the spin−lattice relaxation rates of substrate nuclei due to dipolar interactions with the paramagnetic cation (*1*−*6*). ^{31}P relaxation measurements of this kind have been published for various phosphoryl transfer enzymes to determine the location of the cation, Co(II), with respect to the phosphate chain (*7*−*10*). Further measurements for gathering structural data for nuclei on the adenosine moiety were discouraged by the need to label the carbon and nitrogen nuclei in adenosine with ^{13}C and ^{15}N, respectively. Thus, with the exception of one set of published measurements made on [2-^{13}C]ATP and [2-^{13}C]ADP bound to creatine kinase (*11*), no structural data are available regarding the relative orientation of the phosphate chain with respect to the adenosine for the nucleotide complexes of any of the ATP-utilizing enzymes. This situation was alleviated recently by the fact that nucleotides uniformly labeled with ^{13}C and ^{15}N have become commercially available.

Free in solution, ATP and ADP are floppy molecules with two internal mobilities with large amplitudes and low activation energies, viz., the glycosidic rotation of the adenine with respect to the ribose, and the reorientation of the phosphate chain with respect to the adenosine moiety, in addition to the low-amplitude ribose pucker. If it is assumed that the enzyme-bound nucleotide has a single conformation (*12*), the characterization of such a conformation requires knowledge of a sufficient number of distances between the cation, which is chelated to the phosphate chain, and the nuclei in the adenosine moiety. The availability of [U-^{13}C]-nucleotides makes it possible to acquire the requisite amount of distance data. Furthermore, these distances are expected to be in the range of 5−12 Å so that relaxation times will be longer than the lifetimes of the paramagnetic complexes with Mn(II) as the cation. This circumstance allows evalu-

† Supported in part by the National Institutes of Health (Grant GM43966) and Indiana University−Purdue University Indianapolis (IUPUI). Some of these results were presented at the 39th Experimental NMR Conference (ENC) held at Asilomar, CA, March 22−27, 1998.

* To whom correspondence should be addressed. Phone: (317) 274-6897. Fax: (317) 274-2393. E-mail: brao@iupui.edu.

‡ Permanent address: National Institute of Immunology, Aruna Asaf Ali Marg, New Delhi 1100 67, India.

10.1021/bi991382s CCC: $18.00
Published on Web 11/05/1999

ation of the distances with precision since the theoretical basis for paramagnetic relaxation effects, as well as the procedure for determining the spectral densities entering the theory, is appropriate for Mn(II), in contrast with the situation for Co(II) (*7*). This paper reports a complete set of ^{13}C relaxation measurements made on [U-^{13}C]ATP and [U-^{13}C]ADP bound to yeast PGK[1] at three distinct ^{13}C NMR frequencies: 75.4, 125.7, and 181 MHz. The ^{13}C resonances are well-resolved, and analysis of the measurements yields distances of all 10 ^{13}C nuclei from the cation in each nucleotide complex. The distance data taken along with the previously determined location of the cation with respect to the phosphate chain (*9*) lead, for the first time, to a complete characterization of the structures of enzyme-bound metal−nucleotide complexes.

PGK (EC 2.7.2.3, monomer, molecular mass of 47 kDa) catalyzes the reaction

$$\text{ADP} + \text{1,3-diphosphoglycerate} \overset{\text{M(II)}}{\rightleftharpoons} \text{ATP} + \text{3-P-glycerate}$$

which is the first of two steps of manufacturing ATP in universal anaerobic glycolysis (*13*). M(II) is the obligatory cation. The catalytic equilibrium constant of the reaction predominantly favors ATP formation over the reaction in the reverse direction. However, with stoichiometric enzyme concentrations, the enzyme-bound substrates interconvert with an equilibrium constant approximately equal to unity (*14*). The enzyme is known to bind a second ATP (or ADP) molecule of unknown function in addition to the one at the active site. This ancillary ATP (or ADP) is found to bind the activating cation an order of magnitude weaker than at the catalytic site (*14*−*17*). The contrasting affinities of the cation binding at the two sites guarantee that the paramagnetic relaxation measurements made with a cation−nucleotide concentration ratio of <0.1 exclusively yield distance data for ATP at the active site.[2]

TRNOESY measurements with ATP (ADP) or Mg·ATP (Mg·ADP) in the presence of the enzyme allow the determination of interproton distances in the adenosine moiety of the enzyme-bound nucleotides. Such TRNOESY measurements were useful in ascertaining the glycosidic torsion angles and ribose puckers characterizing adenosine conformations for some ATP-utilizing enzymes (*19*−*23*). However, these experiments could not be performed for PGK because the presence of the second nucleotide binding site on the enzyme complicates the analysis of TRNOESY data. Nevertheless, the ability to determine 10 different ^{13}C distances from the adenosine to the paramagnetic cation is expected to provide adequate data for determining the complete conformation of the bound nucleotide at the active site.

The NMR-determined chelate structure of the cation with the phosphate chain (*9*) of enzyme-bound ATP disagreed with the then available X-ray structure of Mg·ATP- and Mn·ATP-containing crystals of PGK (*24*−*26*). This discrepancy was ascribed to the presence of high concentrations of the anion SO_4^{2-} in the protein crystals grown in ammonium sulfate (*9*, *17*). Several high-resolution X-ray structures have been recently published for crystals of PGK, from *Bacillus stearothermophilus* containing Mg·ADP (*27*), from porcine muscle containing both Mn·AMPPNP and 3-P-glycerate (*28*), and from *Trypanosoma brucei* containing Mg·AMPPNP (*29*−*33*). These structures and subsequent modeling (*30*−*33*) suggest a position for the cation with respect to the nucleotide phosphates different from that proposed earlier (*24*−*26*). Thus, there appears to be uncertainity about the location of the cation with respect to the two substrates in the X-ray structures. Through ^{13}C spin−lattice relaxation measurements presented here, we provide definitive information about the location of the cation with respect to the nucleotide substrate. These results, taken along with the X-ray-determined protein conformation, might allow an incisive evaluation of the structural features that are relevant to the elucidation of the mechanism of the enzyme.

EXPERIMENTAL PROCEDURES

Materials. PGK was isolated from yeast by the method of Fifis and Scopes (*34*). The protein was purified further by Sephadex G-75 gel filtration. The resulting enzyme typically had an activity of ∼1000 units/mg at 22 °C in a coupled assay with glyceraldehyde-3-phosphate dehydrogenase (*35*). For NMR measurements, the protein was dialyzed against Chelex-100 (Bio-Rad) in 200 mM Hepes (partially in D_2O) at pH 8.0 and concentrated to between 5 and 6 mM in an Amicon concentrator with a YM-10 membrane.

[U-^{13}C]ATP was purchased from Isotec. However, this nucleotide required further purification by solid-phase extraction on a SAX column purchased from Varian Sample Preparation Products. [U-^{13}C]ADP prepared from [U-^{13}C]-ATP by using the hexokinase reaction was purified by the same method. With a stepwise salt gradient of 10 to 200 mM ammonium bicarbonate (pH 8.0), AMP elutes first and ATP last. Fractions were checked by NMR as well as by optical absorption at 259 nm. Separated adenine nucleotides were processed individually by repeated rotovaporation with 5−10 additions of 2 mL portions of methanol to decompose the ammonium bicarbonate followed by passage through a Chelex-100 (Bio-Rad) column to remove metal ion contamination. The purity was then checked by ^{31}P NMR.

Samples for NMR experiments typically contained the enzyme at a concentration of 5−6 mM, and the nucleotide concentrations were usually 70−80% of the enzyme concentration. Stock solutions of $MnCl_2$ from Sigma Chemical Co. were diluted to the desired concentrations before being added to the sample mixture described above. The value of [Mn(II)]/[nucleotide] typically varied from 0.005 to 0.05.

Hepes was purchased from Research Organics and D_2O from Cambridge Isotope Laboratories. Other chemicals were reagent grade.

NMR Measurements. ^{13}C NMR measurements at 75.4 and 125.7 MHz were taken on Varian UNITY-300 and INOVA-500 NMR spectrometers equipped with high-stability vari-

[1] Abbreviations: AMPPNP, 5′-adenylyl imidodiphosphate; [U-^{13}C], uniformly labeled with ^{13}C; E·M·S, enzyme·metal·substrate; E·S, enzyme·substrate; Hepes, *N*-(2-hydroxyethyl)piperazine-*N*′-2-ethanesulfonic acid; NMR, nuclear magnetic resonance; PDB, Protein Data Bank; PEG, poly(ethylene glycol); PGK, 3-phosphoglycerate kinase; SAX, strong anion exchange; TRNOESY, two-dimensional transferred nuclear Overhauser effect spectroscopy.

[2] The dissociation constants for nucleotide binding at the catalytic site in the absence of the cation are estimated to be in the range of 50−100 μM with ADP binding more strongly than ATP (*16*, *17*), and in the presence of the cation, the affinity is enhanced several-fold (*18*). The binding at the second site is an order of magnitude weaker.

able-temperature controllers. Typical sample volumes were 2 mL, and all the experiments on enzyme complexes were performed at 5 °C. Experiments at 181 MHz were performed on a similarly equipped Varian UNITYplus-720 NMR spectrometer at the National High Magnetic Field Laboratory in Tallahassee, FL.

Molecular Modeling. Molecular modeling was performed using the CHARMm program (*36*) in the software package Quanta (version 4.1) running on a Silicon Graphics computer. The set of Mn−^{13}C distances obtained have been applied as constraints to an arbitrary initial nucleotide conformation, and the energy of the resultant structure was minimized by molecular mechanics. This energy-minimized structure was then subjected to a conformational search by a grid scan method to determine the acceptable ranges for the dihedral angles characterizing its conformation, by changing the angles in steps of 1°. A narrow range of lowest-energy conformations that are compatible with the NMR-determined distances was thus selected. In an independent procedure, molecular dynamics simulations for times ranging from 1 ps to 1 ns were used. The arbitrary initial nucleotide conformation was equilibrated at 300 K before running the dynamics. In each run, structures at different time intervals were chosen and were subjected to the distance constraints and energy minimization. A convergence of the structures obtained for simulations made for different durations with the range of structures determined by the molecular mechanics procedure described above indicates that a single conformation characterizes the enzyme-bound nucleotide.

THEORY

Relaxation Rates in the Presence of Paramagnetic Cations, Basic Equations. A detailed description of the theoretical basis and experimental strategy used in the measurement of nuclear spin relaxation rates in the presence of paramagnetic cations has been presented previously (*7*−*11*). The equations and derivations specific to this work are presented below. Given our sample conditions, which contain exchanging paramagnetic (E·M·S) and diamagnetic (E·S) complexes in fractional concentrations of p and $1 - p$, respectively, such that $p \ll 1$, the observed relaxation rate $(T_{1,obs})^{-1}$ is given by the sum of the relaxation rate in E·S, $(T_{1D})^{-1}$, and a paramagnetic contribution, $(T_{1P})^{-1}$, as

$$(T_{1,obs})^{-1} = (T_{1D})^{-1} + (T_{1P})^{-1} \quad (1)$$

with

$$(T_{1P})^{-1} = p/(T_{1M} + \tau_M) \quad (2)$$

where τ_M is the lifetime of the paramagnetic complex[3] and $(T_{1M})^{-1}$ is the relaxation rate in the paramagnetic (E·M·S) complex, such that $(T_{1M})^{-1} \gg (T_{1D})^{-1}$. $(T_{1M})^{-1}$ is related to the cation−nucleus distance r(Mn−^{13}C) by

$$(T_{1M})^{-1} = (C/r)^6 f(\tau_C) \quad (3)$$

where

$$C = [(2/15)S(S+1)g^2\gamma_I{}^2\beta^2]^{1/6} \quad (4)$$

and

$$f(\tau_C) = 3\tau_C/(1 + \omega_I{}^2\tau_C{}^2) \quad (5)$$

where S and g represent the spin and the isotropic g-factor of the cation in the E·M·S complex, respectively, β is the Bohr magneton, and γ_I and ω_I are the gyromagnetic ratio and Larmor frequency of the nucleus, respectively. For Mn(II)−^{13}C dipole−dipole interactions, $C = 512$ Å $s^{-1/3}$. $f(\tau_C)$ is a spectral density at ω_I, and τ_C is the correlation time modulating the Mn(II)−^{13}C dipolar interactions, given by

$$\tau_C{}^{-1} = \tau_R{}^{-1} + \tau_{S1}{}^{-1} \quad (6)$$

where τ_R is the rotational correlation time of the E·M·S complex (assumed isotropic) and τ_{S1} is the longitudinal relaxation time of the paramagnetic cation in the complex, given by

$$\tau_{S1}{}^{-1} = B[\tau_V/(1 + \omega_S{}^2\tau_V{}^2) + 4\tau_V/(1 + 4\omega_S{}^2\tau_V{}^2)] \quad (7)$$

in which B is a constant proportional to the square of the fluctuations in the strength of the crystal field interaction implicit in the chelation of the cation, τ_V is the correlation time characterizing such fluctuations, and ω_S is the EPR frequency of the cation.

Equations 2−5 show that

$$(pT_{1P}) - \tau_M = T_{1M} = \left(\frac{r}{C}\right)^6 \frac{1}{f(\tau_C)} = \left(\frac{r}{C}\right)^6 \left[\frac{1}{3\tau_C} + \omega_I{}^2\left(\frac{\tau_C}{3}\right)\right] \quad (8)$$

$f(\tau_C)$ depends on frequency (ω_I) explicitly as given by eq 5 (unless $\omega_I\tau_C \ll 1$) and implicitly through the possible contribution of τ_{S1} to τ_C (see eq 6), since τ_{S1} depends on frequency as given by eq 7. If $\omega_S\tau_V \ll 1$, τ_{S1} is independent of frequency and is given by

$$\tau_{S1}{}^{-1} = 5B\tau_V \quad (9)$$

Therefore, with τ_{S1} given by eq 9, τ_C (given by eq 6) becomes frequency-independent, and a plot of (pT_{1P}) versus $\omega_I{}^2$, as given by eq 8, will be linear with a slope equal to $(r/C)^6 \cdot (\tau_C/3)$ and an intercept given by $[\tau_M + (r/C)^6(1/3\tau_C)]$. On the other hand, if $\omega_S\tau_V \gg 1$, eq 7 reduces to

$$\tau_{S1} = \tau_V\omega_S{}^2/2B = A\omega_I{}^2 \quad (10)$$

where

[3] τ_M is actually an "effective" lifetime to which all the dissociation and association steps implicit in S exchanging between E·S and E·M·S complexes contribute. This exchange can be initiated by three distinct paths, viz., E·M·S ↔ E + M·S, E·M·S ↔ E·M + S, and E·M·S ↔ E·S + M. The relative importance of these processes depends, in general, on the specific enzyme, substrate, and cation in the complex being investigated. For nucleotide complexes of kinases studied thus far, the rate-determining process appears to be E·M·S ↔ E + M·S ↔ E + M + S ↔ E·S. Although multiple steps and paths contribute to the exchange, for the purpose of calculating the nuclear spin relaxation rate $(T_{1P})^{-1}$ observed for the composite system at equilibrium, a binary exchange process involving E·M·S and E·S with an effective lifetime τ_M for E·M·S is appropriate. The binary exchange is represented by a 2 × 2 determinant, the roots of which are the relaxation rates. In the limit $p \ll 1$ and $T_{1M} \ll T_{1D}$, the faster of these rates is virtually unobservable and the slower rate, given by eqs 1 and 2, is the observed relaxation rate.

$$A = \frac{\tau_V}{2B}\left(\frac{g\beta}{\gamma_I}\right)^2 \quad (11)$$

τ_{S1}, and therefore τ_C (see eq 6), are now frequency-dependent. A plot of (pT_{1P}) versus ω_I^2, as given by eq 8, will then be nonlinear.

Measurements of T_{1P} as a function of ω_I (for at least three different values) are typically needed to quantitate $f(\tau_C)$ in eq 3 and estimate τ_M, before evaluation of r[Mn(II)−^{13}C] for any given nucleus.

Deduction of $f(\tau_C)$ and τ_M from Multiple Relaxation Rates. A feature of the results presented here, which did not occur in previous analyses of paramagnetic relaxation rate measurements in enzyme-bound complexes, is that the data are simultaneously gathered for 10 different ^{13}C nuclei in the complex. It is, therefore, necessary to determine one set of values for $f(\tau_C)$ and τ_M that are compatible with the data for all the nuclei. This procedure is simplified by noting that a plot of $(pT_{1P})_1$ values obtained for all the nuclei at $\omega_I = \omega_1$ versus the $(pT_{1P})_2$ values obtained at $\omega_I = \omega_2$ is a straight line, independent of r, as shown by substituting eq 5 and eq 3 into eq 2

$$\frac{(pT_{1P})_1 - \tau_M}{(pT_{1P})_2 - \tau_M} = \frac{(T_{1M})_1}{(T_{1M})_2} = [(1 + \omega_1^2\tau_{C1}^2)/(1 + \omega_2^2\tau_{C2}^2)](\tau_{C2}/\tau_{C1}) \quad (12)$$

where τ_{C1} and τ_{C2} are the values of τ_C, and $(T_{1M})_1$ and $(T_{1M})_2$ are the values of T_{1M}, at frequencies ω_1 and ω_2, respectively.

To proceed further with the analysis, the two cases discussed above regarding the frequency dependence of pT_{1P}, viz. the plots of pT_{1P} versus ω_I^2 being linear and pT_{1P} versus ω_I^2 being nonlinear, should be considered. If the plot of pT_{1P} versus ω_I^2 is linear, i.e., when τ_C is independent of frequency, so that $\tau_{C1} = \tau_{C2} = \tau_C$, then the slope, R, of the linear plot of $(pT_{1P})_1$ versus $(pT_{1P})_2$ is given by

$$R(\omega_1,\omega_2) = \frac{1 + \omega_1^2\tau_C^2}{1 + \omega_2^2\tau_C^2} \quad (13)$$

and it may be seen that

$$\tau_C = [(1 - R)/(R\omega_2^2 - \omega_1^2)]^{1/2} \quad (14)$$

and

$$\tau_M = \text{intercept}/(1 - R) \quad (15)$$

On the other hand, if the plot of pT_{1P} versus ω_I^2 is nonlinear, i.e., when τ_C is frequency-dependent, eqs 13−15 are not applicable (although eq 15 is still valid) because the slope is now given by the right-hand side of eq 12 in which τ_{C1} and τ_{C2} are contributed by a frequency-dependent τ_{S1}. For example, when $\omega_S\tau_V \gg 1$, and if τ_S is sufficiently shorter than τ_R so that $\tau_C \simeq \tau_{S1}$ at both frequencies, the slope, R', of a plot of $(pT_{1P})_1$ versus $(pT_{1P})_2$ is obtained by the use of eqs 9−11 as

$$R'(\omega_1,\omega_2) = [(1 + A^2\omega_1^6)/(1 + A^2\omega_2^6)]\omega_2^2/\omega_1^2 \quad (16)$$

In this case, the values of B and τ_V (and, therefore, the value of τ_S as a function of frequency) can be obtained by fitting the slopes, $R'(\omega_1,\omega_2)$, for different values of ω_1 and ω_2 to eqs 10−12 and 16 with the help of a computer program.

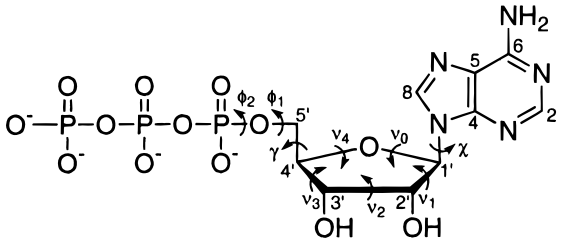

FIGURE 1: Model of free ATP with atom numbering. Curved arrows show the dihedral angles that characterize the nucleotide conformation. The cation which would be bound to the phosphates is not shown.

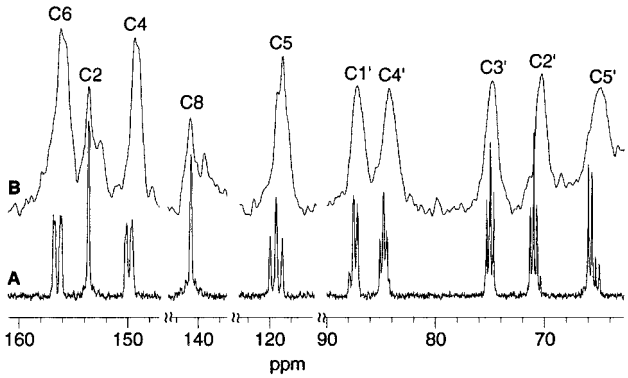

FIGURE 2: Proton-decoupled ^{13}C NMR spectra of [U-^{13}C]ATP (A) and E·[U-^{13}C]ATP (B) at 125.7 MHz. Sample conditions were as follows: (A) 6.3 mM ATP in 50 mM K-Hepes at pH 8.0 and 22 °C or (B) 6.4 mM enzyme, 3.9 mM [U-^{13}C]ATP, and 50 mM K-Hepes at pH 8.0 and 5 °C. NMR parameters were as follows for panel A: number of data points, 8192; sweep width, 25 999 Hz; 432 scans; recycle delay, 5 s; and line broadening, 3 Hz. Those for panel B were the same as those for panel A except the number of scans (64) and line broadening (40 Hz).

RESULTS AND ANALYSIS

^{13}C NMR Spectra of [U-^{13}C]ATP and E·[U-^{13}C]ATP. A schematic of the ATP structure, with the numbering of the ^{13}C-labeled sites indicated, is shown in Figure 1. Proton-decoupled ^{13}C NMR spectra of [U-^{13}C]ATP and E·[U-^{13}C]-ATP at pH 8.0 and 5 °C recorded at 125.7 MHz shown juxtaposed in panels A and B of Figure 2, respectively, indicate that the 10 different ^{13}C resonances of the labeled nucleotide are clearly identifiable. The labeling of the various resonances is based on the previously published assignment of the resonance (*37*). The ^{13}C−^{13}C spin couplings between adjacent ^{13}C nuclei are all resolved in the spectrum of the free nucleotide (Figure 2A), with values of ∼40 Hz for the ribose carbons and ∼50−70 Hz for the adenine base carbons. In the enzyme-bound complex, all the resonances were broadened enough to make the spin−spin couplings unresolvable, with line widths varying from 110 to 280 Hz. It may also be seen from panels A and B of Figure 2 that the ^{13}C resonances of the bound complex exhibit negligible chemical shifts (<1 ppm) with respect to those for the free nucleotide. The spectra were qualitatively similar for [U-^{13}C]-ADP and E·[U-^{13}C]ADP.

Relaxation Measurements. The nuclear spin relaxation rates of ^{13}C nuclei in the [U-^{13}C]ADP and [U-^{13}C]ATP bound

Table 1: Paramagnetic Effect (pT_{1P}) in Milliseconds Due to Mn(II) on ^{13}C Relaxation Rates for E·Mn·[U-^{13}C]ADP and E·Mn·[U-^{13}C]ATP Complexes of Yeast PGK[a]

	pT_{1P} for E·Mn·[U-^{13}C]ADP (ms)			pT_{1P} for E·Mn·[U-^{13}C]ATP (ms)		
carbon	75.4 MHz	125.7 MHz	181 MHz	75.4 MHz	125.7 MHz	181 MHz
C2	5.9	13.6	28.4	7.2	15.5	37.4
C4	8.1	19.9	34.4	7.9	11.8	21.5
C5	6.5	14.1	27.5	2.9	4.6	10.0
C6	6.4	11.9	21.5	4.9	8.6	17.5
C8	3.6	7.7	13.8	1.9	3.1	4.7
C1′	14.0	39.9	46.0	12.8	16.6	45.6
C2′	9.1	20.9	34.1	7.0	10.2	28.7
C3′	9.4	35.7	43.3	8.2	14.4	30.6
C4′	14.0	20.4	24.0	9.6	9.0	19.9
C5′	3.1	5.1	10.2	3.3	3.4	8.4

[a] The experimental (NMR) error in the T_1 values is ±5%. At each frequency, measurements were taken for five to seven different values of p (=[M]/[S]). p values that were typically used were between 1 and 5%. Protein and nucleotide concentrations were 4−6and 2.5−4.1 mM, respectively.

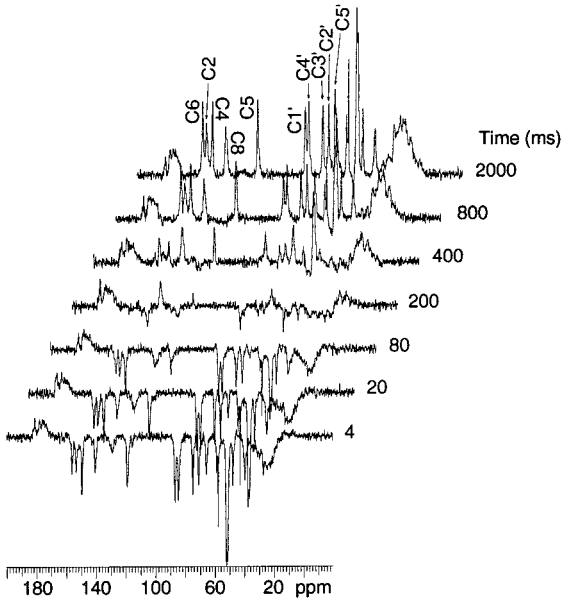

FIGURE 3: Proton-decoupled ^{13}C T_1 stack plot, obtained at 181 MHz with an inversion−recovery sequence, for E·[U-^{13}C]ATP in the presence of Mn(II). NMR parameters were as follows: number of data points, 8192; sweep width, 39 841 Hz; 40 scans; recycle delay, 4 s; and line broadening, 20 Hz. The recovery delay times are the labels for the spectra. Sample conditions were as follows: 6.4 mM enzyme, 2.72 mM ATP, and 0.08 mM $MnCl_2$ at 5 °C. The carbon atom numbering corresponds to that given in Figure 1.

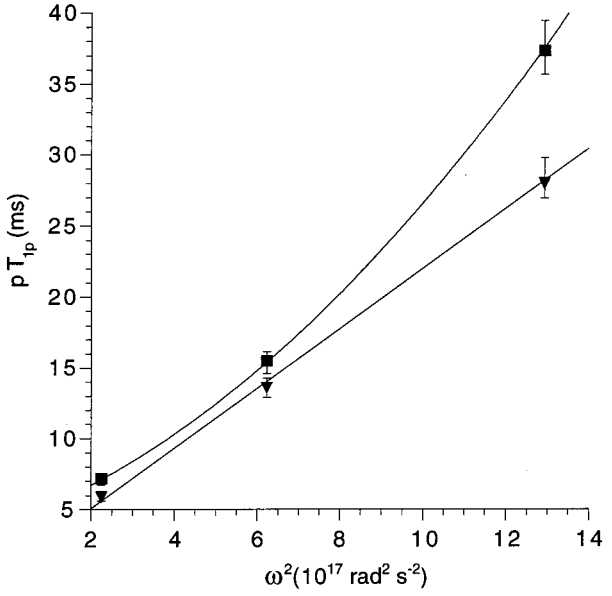

FIGURE 4: Variation of the relaxation rates (pT_{1p}) vs the square of the NMR frequencies (ω_I^2) for C2 in E·Mn·[U-^{13}C]ATP (■) and E·Mn·[U-^{13}C]ADP (▼). Experimental data shown by the solid points are for 75.4, 125.7, and 181 MHz. Solid curves are drawn with theoretically calculated values for each nucleotide complex. For E·Mn·[U-^{13}C]ADP, the parameters were as follows: $r = 8.6$ Å and $B\tau_V = 6.34 \times 10^7$ s^{-1}. For E·Mn·[U-^{13}C]ATP, they were as follows: $r = 8.9$ Å and $\tau_V/B = 8.1 \times 10^{-34}$ s.[3]

to PGK were measured as a function of added $MnCl_2$ concentration to determine $(pT_{1P})^{-1}$ from the slope of the p dependence of $(T_{1,obs})^{-1}$. On the basis of both measured (*16*) and estimated (*17*) dissociation constants,[2] at the concentrations of PGK and nucleotides used in the experiments, more than 97% of the cation-bound nucleotides exist in enzyme-bound complexes (*9*). A typical T_1 stack plot is shown in Figure 3. In the two cases where there is overlap between the signals (between C6, C2, and C4 of the adenine moiety, and between C1′ and C4′ of the ribose moiety), deconvolution procedures, available in the data processing program VNMR, on the Varian spectrometer were used to delineate the T_1 values of the individual resonances. The ^{13}C relaxation times, pT_{1P}, measured at three different frequencies are given in Table 1 for both E·Mn·ADP and E·Mn·ATP. Plots of pT_{1P} versus ω_I^2 for C2 in the two complexes, shown in Figure 4, indicate that the magnitude and frequency dependence of the ^{13}C relaxation rates in the bound nucleotide are markedly different in E·Mn·[U-^{13}C]ADP and E·Mn·[U-^{13}C]ATP. For the ADP complex, the plot is linear whereas for the ATP complex, there is significant curvature in the plot. All carbons behaved in a similar fashion (plots not shown). This result is similar to that seen for creatine kinase complexes with [2-^{13}C]ADP and [2-^{13}C]ATP (*11*). The linear dependence of pT_{1P} on ω_I^2 in the case of E·Mn·[U-^{13}C]ADP suggests that τ_C is independent of frequency in this case (see eq 9), whereas the nonlinearity of the plot of pT_{1P} versus ω_I^2 in the case of E·Mn·[U-^{13}C]ATP suggests that τ_C, and therefore τ_S, depend on frequency for this complex (eq 10).

Further analysis of the data was performed on the basis of slopes and intercepts of linear plots of $pT_{1P}(\omega_1)$ versus $pT_{1P}(\omega_2)$ for all the ^{13}C nuclei, which are independent of the ^{13}C−cation distances, as discussed above in the theory section. Examples of linear plots of pT_{1P}(181 MHz) versus pT_{1P}(125.7 MHz) are shown in panels A and B of Figure 5 for E·Mn·[U-^{13}C]ATP and E·Mn·[U-^{13}C]ADP, respectively.

Table 2: Mn(II)−^{13}C Distances for the Labeled Carbons in the Nucleotides Calculated Using eqs 3−6 with a C of 512 Å $s^{-1/3}$, a τ_C of 2.8 ns for E·ADP Independent of Frequency, and τ_C Values of 0.6, 1.6, and 3.1 ns for E·ATP at 75.4, 125.7, and 181 MHz, Respectively[a]

carbon	E·[U-^{13}C]ADP (Å) (NMR) (±0.5)	E·[U-^{13}C]ADP (Å) (model)	E·Mg·ADP[b] (Å) (X-ray)	E·[U-^{13}C]ATP (Å) (NMR) (±0.5)	E·[U-^{13}C]ATP (Å) (model)	E·Mg·ATP[c] (Å) (X-ray)
C2	8.6	9.1	11.5	8.9	9.0	12.7
C4	8.8	8.6	9.9	8.3	8.1	11.0
C5	8.3	8.1	11.0	7.2	7.3	11.9
C6	8.0	8.1	12.3	7.9	7.7	13.1
C8	7.4	7.6	9.4	6.4	6.7	10.2
C1′	9.3	8.7	7.5	9.1	9.0	8.6
C2′	8.8	8.6	7.4	8.4	8.6	8.0
C3′	9.2	8.8	6.0	8.7	8.6	7.2
C4′	8.5	8.2	5.3	8.1	8.2	6.7
C5′	6.8	6.6	4.9	6.9	6.7	7.0

[a] Distances that are given are averages of those obtained for the data at the three frequencies. Distances for the model were derived from the final minimized structures and were within ±0.2 Å. The corresponding distances for the E·Mg·ADP and E·Mg·ATP complexes are from published X-ray structures downloaded from the Protein Data Bank. [b] PDB file name 1PHP (*27*). PDB file name 13PK (*29*). [c] PDB file name 3PGK (*26*).

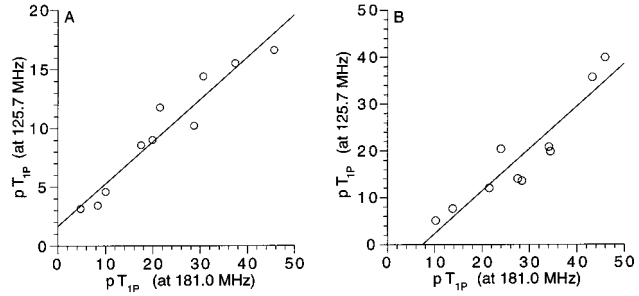

FIGURE 5: pT_{1P} at 181 MHz vs pT_{1P} at 125.7 MHz for E·Mn·[U-^{13}C]ATP (A) and E·Mn·[U-^{13}C]ADP (B).

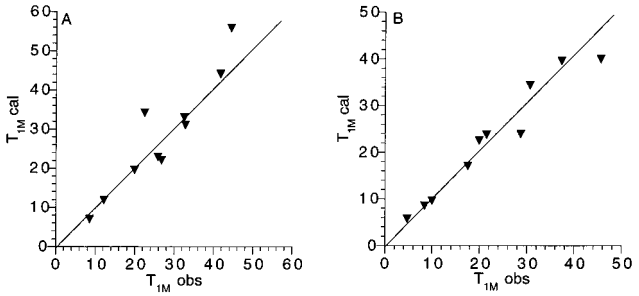

FIGURE 6: Typical plot of observed T_{1M} values vs calculated T_{1M} values. Data are shown for 181 MHz for (A) E·Mn·[U-^{13}C]ADP and (B) E·Mn·[U-^{13}C]ATP. Parameters used for the back-calculation using eqs 2−7 were, the r values for each carbon given in Table 2, a C of 512 Å $s^{-1/3}$, and B and τ_V values given in the legend of Figure 4. The solid line through the origin is drawn with a slope of 1.

The ω_S values for Mn(II) corresponding to the three ^{13}C frequencies employed, viz., 75.4, 125.7, and 181 MHz, are 1.24×10^{12}, 2.06×10^{12}, and 2.98×10^{12} s^{-1}, respectively. In the case of the E·Mn·[U-^{13}C]ADP complex (Figure 5B), since τ_C is independent of frequency, as discussed above, the slope and intercept are given by eqs 13−15. Analysis on this basis yields a τ_M value of 1.6 ms and a τ_C ($=\tau_S$) value of 2.8 ns, independent of frequency. This value of τ_C corresponds to $B\tau_V = 6.34 \times 10^7$ s^{-1}, with a τ_V of $\leq 10^{-13}$ s ($B \geq 6 \times 10^{20}$ s^{-2}) to satisfy the requirement that $(\omega_S\tau_V)^2 \ll 1$ to make τ_S frequency-independent (see eqs 7 and 9). On the other hand, for the E·Mn·[U-^{13}C]ATP complex, the nonlinear dependence of pT_{1P} on ω_I^2 arises from the frequency dependence of τ_S as shown above, and eqs 10, 12, and 16 are appropriate. The slopes and intercepts of the three $pT_{1P}(\omega_1)$ versus $pT_{1P}(\omega_2)$ plots were fitted to these equations with the help of a computer program. This gave a value of 0.9 ms for τ_M and a τ_V/B of 8.1×10^{-34} s^3 where $\tau_V \geq 2.5 \times 10^{-12}$ s ($B \geq 3 \times 10^{21}$ s^{-2}) to satisfy the requirement that $\omega_S\tau_V \gg 1$ implicit in eqs 10 and 12. Substituting in eq 10 gives τ_C ($=\tau_S$) values of 0.6, 1.6, and 3.1 ns at ^{13}C frequencies of 75.4, 125.7, and 181 MHz, respectively. For both E·Mn·ADP and E·Mn·ATP, $\tau_C \approx \tau_S$ since τ_R for PGK is about 25 ns, which is 1 order of magnitude larger than the values of τ_S deduced above (see eq 6). The contrasting frequency dependence of pT_{1P} is thus due to the very different values for the parameters B, τ_V, and τ_S for the ADP and ATP complexes. The τ_M values of 1.6 and 0.9 ms determined for E·Mn·ADP and E·Mn·ATP complexes, respectively, are consistent with the fact that the affinity of ADP for the enzyme is greater than that of ATP both in the presence and in the absence of the cation.

The 10 Mn−^{13}C distances were calculated substituting the measured T_{1M} values and τ_C values deduced above into eq 3. The results are given in Table 2 for both nucleotide complexes. To ascertain the accuracy of the analysis, T_{1M} values were back-calculated, from the values obtained for r, τ_S, B, and τ_V, and compared with the experimental values for all the ^{13}C nuclei at each of the three frequencies. A comparison of the experimental and calculated values for 181 MHz is shown, as a representative example, in panels A and B of Figure 6 for E·Mn·[U-^{13}C]ADP and E·Mn·[U-^{13}C]ATP, respectively. The generally good agreement between observed and calculated T_{1M} values validates the analysis described above.

Structural Characterization. As stated earlier, a detailed molecular structure of the enzyme-bound nucleotides was obtained by using the NMR-determined Mn−^{13}C distances along with previously published cation−^{31}P distances (*9*) as constraints in the Quanta molecular modeling program. Table 2 also gives the distances obtained in the final model and demonstrates the compatibility of the model with the relaxation data. The dihedral angles that characterize nucleotide conformation are the glycosidic torsion χ, the phosphate chain orientation defined by the three rotations γ (O5′−C5′−C4′−C3′), ϕ_1 (C4′−C5′−O5′−Pα), and ϕ_2 (C5′−O5′−Pα−Oαβ) (Figure 1). The glycosidic torsion χ is best determined by TRNOESY data involving the interproton distances between the base and the sugar as demonstrated by published data for other ATP-utilizing enzymes. However, since PGK

Table 3: Various Torsion Angles Characterizing the NMR-Determined Enzyme-Bound Nucleotide Structures Compared with Those from Published X-ray Structures[a]

designation	torsion	[U-^{13}C]ADP (model)	ADP[b] (X-ray)	[U-^{13}C]ATP (model)	ATP[c] (X-ray)
χ	O4′−C1′−N9−C8	33.0	66.9	35.3	−8.5
γ	O5′−C5′−C4′−C3′	50.0	175.4	47.2	−109.3
ϕ_1	C4′−C5′−O5′−Pα	−174.0	119.0	165.7	−83.2
ϕ_2	C5′−O5′−Pα−Oαβ	−70.0	54.8	59.5	−148.5
υ_0	C4′−O4′−C1′−C2′	32.3	−25.5	10.8	2.7
υ_1	O4′−C1′−C2′−C3′	−6.5	37.8	12.9	22.3
υ_2	C1′−C2′−C3′−C4′	−19.6	−34.2	−30.1	31.7
υ_3	C2′−C3′−C4′−O4′	39.4	20.1	36.3	−31.8
υ_4	C3′−C4′−O4′−C1′	−4.1	3.2	−29.9	18.6

[a] The angles were measured from structures obtained by minimization with distance constraints after molecular dynamics for 1 ns. More than 40 structures were analyzed for each nucleotide. The values for the angles in the model were derived from a conformation search on energy-minimized structures. Crystal structure data were obtained from the published structures. The sructures and coordinates were downloaded from the Protein Data Bank. [b] PDB file name 1PHP (*27*). PDB file name 13PK (*29*). [c] PDB file name 3PGK (*26*).

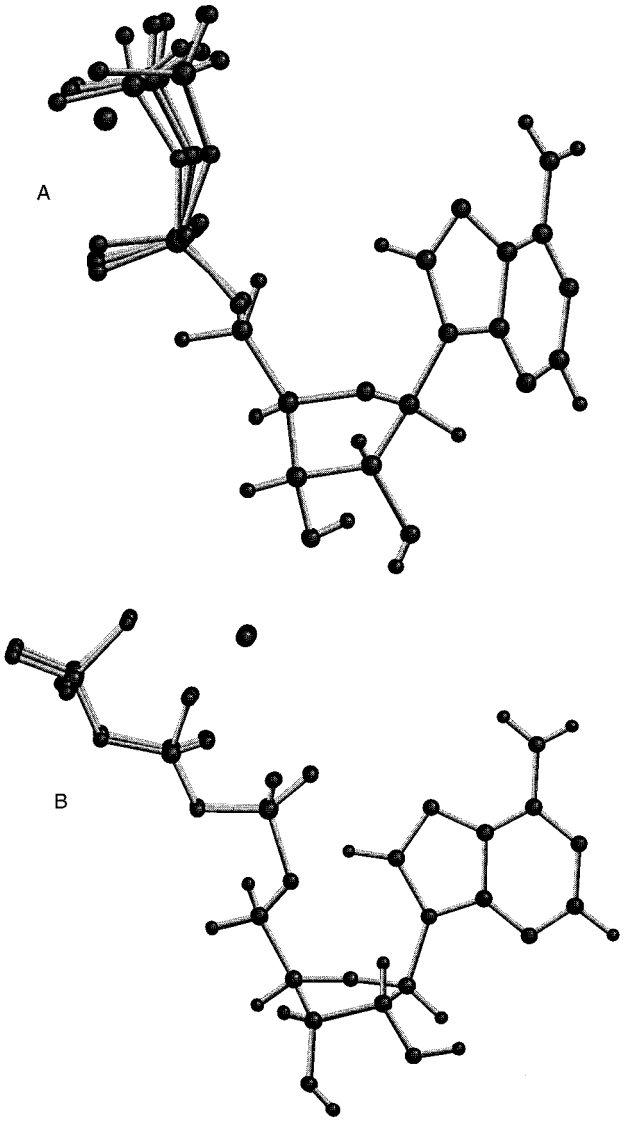

FIGURE 7: Superposition of five structures generated after molecular dynamics and minimization (see the text): (A) E·Mn·ADP and (B) E·Mn·ATP. The cation is shown disjointed from the rest of the nucleotide.

has an ancillary binding site for the nucleotide in addition to the active site, both sites would be occupied at the nucleotide concentrations typically used in TRNOESY experiments (*19*). The TRNOESY data would be a sum of the contributions from the two sites and cannot be analyzed unless the TRNOE data can be independently determined for one of the sites through other means (*20*). Nevertheless, among the Mn(II)−^{13}C distances, χ is sensitive to the Mn−C2 and Mn−C8 distances and to a lesser extent to the Mn−C4 and Mn−C6 distances. These distances were therefore used to find the most acceptable range for χ. A conformation search showed that a χ of 35 ± 10° best fits the distance data for both ADP and ATP. This value, although somewhat lower, overlaps with the general range of 51 ± 7° observed for other ATP-utilizing enzymes (*23*). Detailed molecular dynamics simulations were performed to scan the conformational space for a maximum simulation time of 1 ns. After simulation and energy minimization with the NMR-determined distance constraints, all the lowest-energy structures exhibited χ angles of 32 ± 0.5° and 35 ± 0.5° for ADP and ATP, respectively. Panels A and B of Figure 7 show overlays of some of the structures obtained for ADP and ATP, respectively. There is good convergence for each nucleotide (rms deviation = 0.2−0.4 Å). The various dihedral angles characterizing these structures are listed in Table 3. As we approach the termini of the phosphate chain, the range of acceptable dihedral angle values (for ϕ_3, ϕ_4, and ϕ_5) increases, as is evident by the increasing rms deviation toward the termini. An independent conformational search, made by individually varying the angles γ, ϕ_1, and ϕ_2 from 180° to −180°, to fit the observed Mn−^{13}C distances, agreed well with the values obtained by molecular dynamics.

From Figure 7 and Table 2, it is evident that details of the enzyme-bound ADP and ATP conformations, specified with respect to the cation in the complexes as the origin, are distinguishably different from each other. On the other hand, the position of the cation is displaced by ∼2.4 Å when the adenosine moieties of E·Mn·ADP and E·Mn·ATP are superposed. Similar changes, indicative of structural alterations in enzyme-bound reaction complexes accompanying the enzyme turnover, have been observed for nucleotide complexes bound to rabbit muscle creatine kinase (*11*).

Also given in Table 2 are the distances measured from published X-ray structures corresponding to those determined here, and in Table 3, the various dihedral angles characterizing the X-ray structures are given alongside the corresponding values obtained in the work presented here. It is clear from these data that the NMR-determined structures

differ significantly from those obtained from X-ray crystallography.

DISCUSSION

The paramagnetic relaxation data presented here have been analyzed by considering a single value for $f(\tau_C)$ (see eq 3) at any frequency for all the ^{13}C nuclei. This procedure implicitly assumes that the large-amplitude internal mobilities with low activation energies in free nucleotides, viz., glycosidic reorientation and phosphate chain mobility, have been arrested in their enzyme complexes. Evidence that the glycosidic reorientation is arrested in the enzyme complexes was obtained previously be measuring the rotational correlation times on the basis of the differentially broadened proton-coupled ^{13}C line shapes of [2-^{13}C]ATP bound to various ATP-utilizing enzymes (*12*). Furthermore, TR-NOESY data between the protons of the adenine base and the ribose in the adenosine moieties of Mg·ATP bound at the active sites of a number of these enzymes could be analyzed on the basis of a single conformation in which the glycosidic orientation is well-defined (*19*−*23*). Since Mn(II) is attached to the phosphate chain in the nucleotides, the two results, (i) that the relaxation rates of the 10 ^{13}C nuclei on the adenosine moieties in both E·Mn·ADP and E·Mn·ATP could be evaluated on the basis of a single $f(\tau_C)$ (at each frequency) and (ii) that the $^{13}C-$cation distances obtained could be modeled to yield a single conformation for the bound nucleotide that is not excessively elevated in molecular mechanics energy, indicate that the phosphate chain assumes a unique orientation with respect to the adenosine moiety. It should be noted that if conformational exchange involving significant changes in $^{13}C-$Mn(II) were to occur, the single conformation models from the data would be distorted in view of the strong nonlinearity of the dependence of relaxation rates on the distances (proportional to r^{-6}). Furthermore, it may be argued on general grounds that efficient enzymatic catalysis requires immobilization of the bound substrates, and the results presented here are consistent with this view.

The conformations obtained for E·Mn·ADP and E·Mn·ATP as well as the values of B and τ_V characterizing the electron relaxation of Mn(II) in these two complexes are noticeably different from each other. In both cases, the correlation time, τ_C, modulating the $^{13}C-$Mn(II) dipolar interactions is primarily due to the electronic relaxation times (τ_S) rather than to rotational correlation time τ_R (see eq 6). However, while τ_S for E·Mn·ADP is frequency-independent and $\omega_S\tau_V \ll 1$, for E·Mn·ATP, τ_S is frequency-dependent and $\omega_S\tau_V \gg 1$ in the frequency range of the measurements. This contrasting behavior is clearly due to larger values of B, the strength of the crystal field, and of τ_V, the correlation time for its modulation (see Theory) for E·Mn·ATP relative to those for E·Mn·ADP. The larger value of B for the E·ATP complex may be related to the fact that it is a tridentate complex, whereas E·ADP forms a bidentate complex with the cation. The differences in τ_V are indicative of different rates of modulation of the crystal field due to solvent interactions as well as the association and dissociation processes involving the cation. The results obtained indicate that these processes occur more rapidly in the bidentate (ADP) complex than in the tridentate (ATP) complex. The same contrasting frequency dependence was exhibited by E·Mn·[2-^{13}C]ATP and E·Mn·[2-^{13}C]ADP complexes of rabbit muscle creatine kinase. Whether this behavior is a common feature for all phosphoryl transfer enzymes remains to be seen.

The changes in $^{13}C-$Mn(II) distances between E·Mn·ADP and E·Mn·ATP suggest that significant structural alterations occur in the nucleotide as the reversible phosphoryl transfer takes place on the surface of the enzyme. It should be noted that these changes are specified with respect to a fixed cation. The location of the cation is likely to undergo a movement as the tridentate E·Mn·ATP complex changes to the bidentate E·Mn·ADP complex as the (γ-P)ATP is cleaved and transferred. For example, if the adenosine moieties in the structures derived for E·Mn·ADP and E·Mn·ATP are superposed, the cation is displaced ~2.4 Å between the two complexes. This displacement is larger than the ~1.7 Å previously deduced from relaxation measurements in the presence of Mn(II) on 2-^{13}C-labeled nucleotides bound to rabbit muscle creatine kinase (*11*). Knowledge of the structural alterations accompanying catalytic turnover on the enzyme surface may be useful in visualizing the molecular movements implicit in the catalytic mechanism, and in elucidating the functional roles of the amino acid residues enveloping the substrate at the active site.

With the enzyme-bound nucleotide conformation fully characterized along with the location of the cation, it is proposed to extend the paramagnetic relaxation measurements by using U-^{13}C-labeled 3-P-glycerate. Distance measurements between Mn(II) and ^{31}P(3-P-glycerate) in E·Mn·ADP·3-P-glycerate have been reported previously (*9*). The ^{13}C measurements with the labeled second substrate will thus enable the structural characterization of the entire reaction complex at the active site. These data are expected to shed light on the structural changes in the reaction complex accompanying the hinge bending motion implicated in the mechanism of this enzyme (*33*, *38*).

The NMR-determined conformations of E·Mn·ADP and E·Mn·ATP differ significantly from those derived from X-ray crystallography as reflected both in the cation$-^{13}C$ distances and in the dihedral angles (Tables 2 and 3). In general, the distances of the sugar carbons are shorter and those of the base carbons longer in the X-ray-derived structure than in the NMR-derived structure in both E·Mn·ADP and E·Mn·ATP complexes. Furthermore, the distance differences between ADP and ATP are more pronounced in the X-ray structures (0.6 vs 2.1 Å) than in the NMR structures (0.1 vs 1.1 Å). Details of enzyme-bound nucleotide conformations in the liquid state determined by NMR often disagree with those obtained from crystal structure analysis (*23*). More than a decade ago, it was shown that while EPR (*39*) and NMR (*9*) measurements of ATP complexes yield clear evidence of direct coordination of the cation to all three phosphate groups, the X-ray crystallography results obtained for crystals of PGK soaked with Mg·ATP or Mn·ATP showed coordination of the cation with just the γ-P of ATP (*24*−*26*). One reason that was suggested for the discrepancy was the presence of high concentrations (~2 M) of ammonium sulfate in the crystals that were used (*17*). The recently published crystal structure data of PGK from *T. brucei* with Mg·ADP and Mg·AMPPNP were obtained with crystals grown in 2.5 M potassium sodium phosphate (*29*−*33*). Other recent crystal structures of the Mg·ADP complex of PGK

from *B. stearothermophilus* were obtained with crystals grown in PEG with Mg·ATP which hydrolyzed to Mg·ADP during the course of crystallization (*27*), and the crystal structure data for the Mn·AMPPNP with 3-P-glycerate complex of porcine PGK were obtained with PEG-grown PGK crystals soaked in a 23% PEG solution containing Mn·AMPPNP and 3-P-glycerate (*28*). When the influence of crystal packing effects is considered, and that of the procedures used in crystallization, the disagreement between substrate conformations observed in crystal structures and those determined in the liquid state by methods such as NMR and EPR should not come as a surprise. On the other hand, it should be recognized that crystallography is undeniably one of the most reliable and efficient means for obtaining information about protein structure at the active site. This circumstance, and the availability of sophisticated iterative computer simulation programs, suggest the possibility of combining the strengths of these two powerful structural methodologies by trying to dock NMR-determined substrate structures with the protein structure data obtained through crystallography. We are in the process of making such attempts to obtain what is hoped to be incisive and possibly complete information about the active site structure inclusive of the substrate conformation as well as the protein environment.

ACKNOWLEDGMENT

We thank Dr. Yan Lin for her help with some of the experiments and molecular modeling, Ms. Marina Lyshevski and Ms. Prasanthi Bhagavatula for protein preparation, Dr. Daniel H. Robertson (at the Facility for Computational Molecular Science, Indiana University—Purdue University, Indianapolis) for helpful suggestions, and Dr. Nagarajan Murali for facilitating the measurements at the National High Magnetic Field Laboratory.

REFERENCES

1. Burton, D. R., Forsen, S., Karlstrom, G., and Dwek, R. A. (1979) *Prog. Nucl. Magn. Reson. Spectrosc. 13*, 1−45.
2. Dwek, R. A. (1973) in *NMR in Biochemistry*, Chapters 9 and 10, Clarendon Press, Oxford, U.K.
3. James, T. L. (1975) in *NMR in Biochemistry*, pp 177−210, Academic Press, New York.
4. Jardetzky, O., and Roberts, G. C. K. (1981) in *NMR in Molecular Biology*, Chapter III, Academic Press, New York.
5. Villafranca, J. J. (1984) In *Phosphorous-31 NMR: Principles and Applications* (Gorenstein, D. G., Ed.) pp 155−174, Academic Press, New York.
6. Mildvan, A. S., and Gupta, R. K. (1978) *Methods Enzymol. 49*, 322−359.
7. Jarori, G. K., Ray, B. D., and Nageswara Rao, B. D. (1985) *Biochemistry 24*, 3487−3494.
8. Jarori, G. K., Ray, B. D., and Nageswara Rao, B. D. (1989) *Biochemistry 28*, 9343−9350.
9. Ray, B. D., and Nageswara Rao, B. D. (1988) *Biochemistry 27*, 5579−5585.
10. Ray, B. D., Rösch, P., and Nageswara Rao, B. D. (1988) *Biochemistry 27*, 8669−8676.
11. Ray, B. D., Chau, M. H., Fife, W. K., Jarori, G. K., and Nageswara Rao, B. D. (1996) *Biochemistry 35*, 7239−7246.
12. Nageswara Rao, B. D., and Ray, B. D. (1992) *J. Am. Chem. Soc. 114*, 1566−1573.
13. Scopes, R. K. (1973) in *The Enzymes* (Boyer, P. D., Ed.) 3rd ed., Vol. 8, pp 335−351, Academic Press, New York.
14. Nageswara Rao, B. D., Cohn, M., and Scopes, R. K. (1978) *J. Biol. Chem. 253*, 8056−8060.
15. Larsson-Raznikiewicz, M., and Schierbeck, B. (1977) *Biochim. Biophys. Acta 481*, 283−287.
16. Scopes, R. K. (1978) *Eur. J. Biochem. 91*, 119−129.
17. Ray, B. D., and Nageswara Rao, B. D. (1988) *Biochemistry 27*, 5574−5578.
18. Chapman, B. E., O'Sullivan, W. J., Scopes, R. K., and Reed, G. H. (1977) *Biochemistry 16*, 1005−1010.
19. Murali, N., Jarori, G. K., and Nageswara Rao, B. D. (1993) *Biochemistry 32*, 12941−12948.
20. Jarori, G. K., Murali, N., and Nageswara Rao, B. D. (1994) *Biochemistry 33*, 6784−6791.
21. Murali, N., Jarori, G. K., and Nageswara Rao, B. D. (1994) *Biochemistry 33*, 14227−14236.
22. Jarori, G. K., Murali, N., and Nageswara Rao, B. D. (1995) *Eur. J. Biochem. 230*, 517−524.
23. Murali, N., Lin, Y., Mechulam, Y., Plateau, P., and Nageswara Rao, B. D. (1997) *Biophys. J. 70*, 2275−2284.
24. Bryant, T. N., Watson, H. C., and Wendell, P. L. (1974) *Nature 279*, 14−17.
25. Banks, R. D., Blake, C. C. F., Evans, P. R., Haser, R., Rice, D. W., Hardy, G. W., Merrett, M., and Phillips, A. W. (1979) *Nature 279*, 773−777.
26. Watson, H. C., Walker, N. P. C., Shaw, P. J., Bryant, T. N., Wendell, P. L., Fothergill, L. A., Perkins, R. E., Conroy, S. C., Dobson, M. J., Tuite, M. F., Kingsman, A. J., and Kingsman, S. M. (1982) *EMBO J. 12*, 1635−1640.
27. Davies, G. J., Gamblin, S. J., Littlechild, J. A., Dauter, Z., Wilson, K. S., and Watson, H. C. (1994) *Acta Crystallogr. D50*, 202−209.
28. May, A., Vas, M., Harlos, K., and Blake, C. (1996) *Proteins 24*, 292−303.
29. Bernstein, B. E., Michels, P. A. M., and Hol, W. G. J. (1997) *Nature 385*, 275−278.
30. Bernstein, B. E., and Hol, W. G. J. (1997) *Acta Crystallogr. D53*, 756−764.
31. Chandra, N. R., Muirhead, H., Holbrook, J. J., Bernstein, B. E., Hol, W. G. J., and Sessions, R. B. (1998) *Proteins 30*, 372−380.
32. Bernstein, B. E., Michels, P. A. M., Kim, H., Petra, H., and Hol, W. G. J. (1998) *Protein Sci. 7*, 504−507.
33. Bernstein, B. E., and Hol, W. G. J. (1998) *Biochemistry 37*, 4429−4436.
34. Fifis, T., and Scopes, R. K. (1978) *Biochem. J. 175*, 311−319.
35. Scopes, R. K. (1969) *Biochem. J. 113*, 551−554.
36. Brooks, B. R., Bruccoleri, R. E., Olafson, B. D., States, D. J., Swaminathan, S., and Karplus, M. (1983) *J. Comput. Chem. 4*, 187−217.
37. Jones, A. J., Winkley, M. W., Grant, D. M., and Robins, R. K. (1970) *Proc. Natl. Acad. Sci. U.S.A. 65*, 27−30.
38. Haran, G., Haas, E., Szpikowska, B. K., and Mas, M. T. (1992) *Proc. Natl. Acad. Sci. U.S.A. 89*, 11764−11768.
39. Moore, J. M., and Reed, G. H. (1985) *Biochemistry 24*, 5328−5333.

BI991382S